Kinetostatic design of an innovative Schoenflies-motion generator

Jorge Angeles, Stéphane Caro, Waseem A. Khan, Alexis Morozov

The Kinetostatic Design of an Innovative Schönflies Motion Generator

Jorge Angeles, Stéphane Caro, Waseem Khan, Alexei Morozov
Department of Mechanical Engineering
McGill University
{angeles, caro, wakhan, alexvit}@cim.mcgill.ca

Abstract

In this paper, a novel parallel robot is introduced. The robot, a Schönflies-Motion Generator (SMG), is capable of a special class of motions, namely, those produced with serial robots termed SCARA, an acronym for Selective-Compliance Assembly Robot Arm. These motions involve three independent translations and one rotation about an axis of fixed direction. Such motions are known to form a subgroup of the displacement group of rigid-body motions, termed the Schönflies subgroup. The SMG is composed of two identical four-degree-of-freedom serial chains in a parallel array, sharing one common base and one common moving platform. The proximal module of each chain is active and has two controlled axes, the motors being installed on the fixed base. The links can thus be made light, thereby allowing for higher operational speeds. The distal module, in turn, is passive and follows the motions of its active counterpart, the whole mechanism giving, as a result, a four-degree-of-freedom motion to its end-platform.

Keywords: *Parallel Robot, Manipulator, Kinematics, SCARA, Schönflies displacement subgroup*

1 Historical Note and State of the Art

Most industrial robots have articulated structures of the serial type, where each link is coupled to two other links, except for the end links, which are coupled to one single neighbour. However, these simple, open kinematic chains of multi-axis machines exhibit some drawbacks, mostly due to the *pyramidal effect*: each axis must carry all other axes located upstream in the chain. For this reason, parallel robots have attracted the attention of researchers and end-users. First prototypes of the parallel machines date back to the middle of the 20th century. Gough's machine was built in the early 50s and fully operational in 1954. Stewart produced a paper in 1965 (Stewart, 1965); however, he had never built any real prototype (Bonev, 2003). The history of the development of modern robots with a parallel structure can be traced back to the early eighties (Merlet, 2006). As a milestone in this regard, Karl-Erik Neumann designed and built a new type of machine, the "parallel kinematic robot", in 1987 (Brumson, 2005). In spite of the early invention of parallel robots, they were not used widely until the early 90's, since their architectures demanded sophisticated control not affordable with the computational

means available at the time. After 1992, when Comau Pico launched the first multiprocessor controller, new control systems appeared in the market, capable to run parallel-kinematics machines (PKM). The six-rod machining centers (TM series) of Lapik (Russia) appeared on the market in 1994, and measuring machines of similar kinematics (KIM series) in 1992 (the development of KIMs started in the early 80s) (Lapic, 1994).

Most PKM are based on hexapods, also known as Gough-Stewart platforms (Stewart, 1965). An example of PKM currently used in industry is displayed in Fig. 1.

The most widespread operation of PKMs is machining. This includes milling, cutting, drilling and deburring of sheet and cast metal parts. For example, in 1999 more than two thirds of robotic applications of the Tricept manipulator, a hybrid robot in which a 3-DOF spherical wrist is mounted on the moving platform of a 3-DOF four-legged parallel manipulator (Siciliano, 1999), were in the area of machining, where clients wanted to have 10 μm of repeatability, stiffer links, and higher power.

Moreover, nowadays more and more PKMs are not used independently, but as parts of precise machine-tools. The fact of the matter is that high stiffness and high accuracy are as yet to be realized with PKMs. Other possible applications of PKMs are as medical manipulators, educational test-benches, and pharmaceutical setups.

Parallel manipulators promise some advantages over their serial counterparts. Since PKMs are built with closed-loop chains, the expected result of the parallel design is a robot with higher stiffness, and hence, with increased structural stability. In PKMs there is no need to carry motors, because all drives are installed on the fixed base; as a result, the links can be more compact and lighter. This should allow for shorter cycle times than with serial architectures.

Therefore, in PKMs we should achieve the flexibility of a robot combined with the stiffness of a machine tool. As a consequence, PKMs should have an accuracy comparable with those of CNC machine-tools, but with much less material.

2 The Schönflies-Motion Generator

The Schönflies-Motion Generator (SMG) is an innovative robot, under development at McGill University. The McGill University SMG has two legs, each supplied with four joints. Consequently, it has a smaller number of joints as compared to that in conventional PKMs.

This manipulator is capable of a special class of motions, namely, those produced with manipulators termed SCARA, an acronym for *Selective-Compliance Assembly Robot Arm*. These motions involve three independent translations and one rotation about an axis of fixed direction, similar to the motions undergone by the tray of a waiter. Such motions are known to form a subgroup of the displacement group of rigid-body motions, termed the Schönflies subgroup (Bottema and Roth, 1979; Hervé, 1999; Lee and Hervé, 2005). Besides, (Yang et al., 2001) made a list of four-degree-of-freedom (3-translation and 1-Rotation) parallel robot mechanisms based on single-open-chains, which is not complete, as it does not contain the architecture of the McGill University SMG.

The SMG is a manipulator producing four-degree-of-freedom displacements of a rigid body, its moving platform (Angeles and Morozov, 2003). This set of displacements was first studied by the German mathematician-mineralogist Arthur Moritz Schönflies (1853–1928), who found that these displacements have the algebraic structure of a group. For this reason, the set of

such motions is known to geometers as the Schönflies subgroup of the group of rigid-body displacements.

The SMG is composed of two identical four-degree-of-freedom serial chains in a parallel array, sharing one common base and one common moving platform.

Each serial chain comprises, in turn, two cascaded modules producing, each, a set of two-degree-of-freedom displacements: one rotation about a vertical axis fixed to the base, the *pan motion*, and one rotation about a horizontal axis, the *tilt motion*.

On the one hand, the proximal module is active and has two controlled axes. The motors are installed on the fixed base. The links can thus be made very light, thereby allowing for higher operational speeds. On the other hand, the distal module is passive and follows the motions of its active counterparts, the whole mechanism giving, as a result, a four-degree-of-freedom motion to its end-platform. The prototype of the system is displayed in Fig. 2.

Each leg is driven by a pair of identical motors. The whole mechanism, with the four motors installed either at the ceiling or on the floor, provides a manipulation system with a horizontal end-effector having the motion capability of a SCARA end-effector, thereby giving such a motion to a gripper holding rigidly a tool or a workpiece.

Identical motors performing identical tasks means ease of programming and maintenance as well as equal wear. The location of motors on the base, moreover, allows for lighter links and, as a consequence, higher operation speeds. A planetary gear train is used to drive each leg of the SMG.

3 The Kinematics of the SMG

The kinematic chain of the SMG is shown in Figs. 3 and 4. Apparently, the moving plate $\mathcal{M}$ carrying the operation point P, is coupled to the base frame $\mathcal{F}$ by means of two identical limbs. Each limb, in turn, is a serial chain of the RΠΠΠR (Angeles, 2004) type, with Π indicating a parallelogram linkage playing the role of a kinematic pair, which is termed a Π-joint. We now introduce the notation that will be used throughout this paper. At the outset, all symbols with double subscripts, comprising one Roman and one Arabic numeral, refer to the leg, I or II, and to the corresponding item of the respective leg.

Notation	Description
$\{X, Y, Z\}$	the Cartesian coordinates of the operation point P of the end-effector expressed in the coordinate frame $\mathcal{F}(O_{I0}, \mathbf{i}, \mathbf{j}, \mathbf{k})$
ϕ	angle of rotation of the end-effector about the vertical axis
θ_{Ji}	angle of rotation of the ith joint of the Jth leg, measured according with the right-hand rule, for $i = 1, 2, 3, 4, 5$ and $J = I, II$
$\mathbf{a}_{Jk}$	$\overrightarrow{O_{J(k-1)}O_{Jk}}$, for $k = 1, 2, 3, 4$ and $J = I, II$
$\mathbf{a}_{J5}$	$\overrightarrow{O_{J4}P}$, for $J = I, II$
a_i	the projection of $\mathbf{a}_{Ji}$ onto the $X - Y$ plane, for $i = 4, 5$ and $J = I, II$
b_i	the projection of $\mathbf{a}_{Ji}$ onto the Z axis, for $i = 4, 5$ and $J = I, II$
l_i	$\|\mathbf{a}_{Ji}\|$ for $i = 1, 2, 3, 4, 5$ and $J = I, II$
Continuation in next page	

Notation	Description
R	"radius" of the end effector, i.e., the distance between the operation point and the axis of second revolute joint of each limb
l_0	distance between the two fixed bases (drive-units)

Table 1: Nomenclature

We further define θ_{I1}, θ_{I2}, θ_{II1}, and θ_{II2} as the four actuated-joint angles, while θ_{I3}, θ_{I4}, θ_{II3}, and θ_{II4} are the four passive-joint angles. Correspondingly, $\dot{\theta}_{I1}$, $\dot{\theta}_{I2}$, $\dot{\theta}_{II1}$, and $\dot{\theta}_{II2}$ are the four actuated-joint rates.

Then, from the geometric relationships shown in the above figures, we can obtain the geometric relations for leg I:

$$x = -(l_1 + l_2\cos\theta_{I2} + l_3\cos\theta_{I23})\sin\theta_{I1} - R\sin\phi \tag{1a}$$

$$y = -\frac{l_0}{2} + (l_1 + l_2\cos\theta_{I2} + l_3\cos\theta_{I23})\cos\theta_{I1} + R\cos\phi \tag{1b}$$

$$z = l_2\sin\theta_{I2} + l_3\sin\theta_{I23} + b_4 + b_5 \tag{1c}$$

$$\phi = \theta_{I1} + \theta_{I4} \tag{1d}$$

where

$$\theta_{I23} \equiv \theta_{I2} + \theta_{I3}$$

Similarly, for leg II, we have:

$$x = (l_1 - l_2\cos\theta_{II2} - l_3\cos\theta_{II23})\sin\theta_{II1} + R\sin\phi \tag{2a}$$

$$y = \frac{l_0}{2} - (l_1 - l_2\cos\theta_{II2} - l_3\cos\theta_{II23})\cos\theta_{II1} - R\cos\phi \tag{2b}$$

$$z = l_2\sin\theta_{II2} + l_3\sin\theta_{II23} + b_4 + b_5 \tag{2c}$$

$$\phi = \theta_{II1} + \theta_{II4} \tag{2d}$$

where

$$\theta_{II23} \equiv \theta_{II2} + \theta_{II3}$$

4 The Kinetostatic Design

We understand here under *kinetostatics* the mechanical analysis of rigid-body mechanical systems moving under static, conservative conditions. Kinetostatics is thus concerned with the relations between the feasible twists — point-velocity and angular velocity — and the constraint wrenches — force and moment — pertaining to the various links of a kinematic chain. Kinetostatic design, therefore, refers to the dimensioning of the links under kinetostatic conditions.

4.1 Jacobian Matrices

The kinematic chain of the SMG is shown in Figs. 3 and 4. From Fig. 5, one readily derives

$$\mathbf{p}_I = \mathbf{a}_{I1} + \mathbf{a}_{I2} + \mathbf{a}_{I3} \tag{3a}$$

$$\mathbf{p}_{II} = \mathbf{a}_{II1} + \mathbf{a}_{II2} + \mathbf{a}_{II3} + l_0\,\mathbf{j} \tag{3b}$$

where $\mathbf{p}_I$ and $\mathbf{p}_{II}$ denote the position vectors of point P_I and P_{II}, respectively. Moreover, notice that all vectors of the above equations must be expressed in the same frame; otherwise, the addition would not be possible. Upon differentiating both sides of eq. (3), we obtain

$$\dot{\mathbf{p}}_J = \mathbf{J}_J \dot{\boldsymbol{\theta}}_J \quad , \quad J = I, II \tag{4}$$

where $\dot{\boldsymbol{\theta}}_J$ is the the 3-dimensional *joint-rate vector* of leg J, defined as

$$\dot{\boldsymbol{\theta}}_J = \begin{bmatrix} \dot{\theta}_{J1} & \dot{\theta}_{J2} & \dot{\theta}_{J3} \end{bmatrix}^T \quad , \quad J = I, II \tag{5}$$

and $\mathbf{J}_J$ is its 3×3 *Jacobian matrix*, defined as

$$\mathbf{J}_J = \begin{bmatrix} \mathbf{k} \times \mathbf{r}_{J1} & \mathbf{f}_J \times \mathbf{r}_{J2} & \mathbf{f}_J \times \mathbf{r}_{J3} \end{bmatrix} \quad , \quad J = I, II \tag{6}$$

where $\mathbf{r}_{Ji} = \sum_{k=i}^{3} \mathbf{a}_{Jk}$, $i = 1, 2, 3$, while $\mathbf{k}$ is the unit vector associated with the Z-axis, and $\mathbf{f}_J$ is the unit vector normal to the plane of the Π joints of leg J, $J = I, II$.

In order to derive a dimensionless expression of eq.(4), let us divide it by L, which is a *characteristic length*, as yet to be determined:

$$(\mathbf{k} \times \boldsymbol{\rho}_{J1})\,\dot{\theta}_{J1} + (\mathbf{f}_J \times \boldsymbol{\rho}_{J2})\,\dot{\theta}_{J2} + (\mathbf{f}_J \times \boldsymbol{\rho}_{J3})\,\dot{\theta}_{J3} = \dot{\boldsymbol{\sigma}}_J \tag{7}$$

where

$$\boldsymbol{\rho}_{Ji} \equiv \frac{1}{L}\mathbf{r}_{Ji} \quad , \quad i = 1, 2, 3 \tag{8a}$$

$$\boldsymbol{\sigma}_J \equiv \frac{1}{L}\mathbf{p}_J \quad , \quad J = I, II \tag{8b}$$

In order to eliminate the passive joint rates $\dot{\theta}_{J3}$, $J = I, II$, we cross-multiply both sides of eq.(7) by $\mathbf{f}_J \times \boldsymbol{\rho}_{J3}$ from the left, thereby obtaining

$$\mathbf{v}_J \dot{\theta}_{J1} + \Delta_J \mathbf{f}_J \dot{\theta}_{J2} = (\mathbf{f}_J \times \boldsymbol{\rho}_{J3}) \times \dot{\boldsymbol{\sigma}}_J \tag{9}$$

with

$$\begin{aligned} \mathbf{v}_J &\equiv \begin{bmatrix} (\mathbf{f}_J \times \boldsymbol{\rho}_{J3}) \cdot \boldsymbol{\rho}_{J1} \end{bmatrix} \mathbf{k} - \begin{bmatrix} (\mathbf{f}_J \times \boldsymbol{\rho}_{J3}) \cdot \mathbf{k} \end{bmatrix} \boldsymbol{\rho}_{J1} \\ &\equiv \begin{bmatrix} \mathbf{f}_J,\ \boldsymbol{\rho}_{J3},\ \boldsymbol{\rho}_{J1} \end{bmatrix} \mathbf{k} - \begin{bmatrix} \mathbf{f}_J,\ \boldsymbol{\rho}_{J3},\ \mathbf{k} \end{bmatrix} \boldsymbol{\rho}_{J1} \end{aligned} \tag{10}$$

and

$$\Delta_J \equiv \begin{bmatrix} (\mathbf{f}_J \times \boldsymbol{\rho}_{J3}) \cdot \boldsymbol{\rho}_{J2} \end{bmatrix} \equiv \begin{bmatrix} \mathbf{f}_J,\ \boldsymbol{\rho}_{J3},\ \boldsymbol{\rho}_{J2} \end{bmatrix} \tag{11}$$

From Fig. 6, and the observation that points P and P' lying on a line parallel to the axis of rotation of the Schönflies displacement subgroup, move with the same velocity $\dot{\mathbf{p}}$, we have

$$\dot{\boldsymbol{\sigma}}_J = \dot{\boldsymbol{\sigma}} + \frac{1}{2}\,\dot{\phi}\; s(J)\;\mathbf{k}\times(\boldsymbol{\sigma}_I - \boldsymbol{\sigma}_{II}) \tag{12}$$

with

$$s(J) = \begin{cases} +1 & \text{if} \quad J = I \\ -1 & \text{if} \quad J = II \end{cases} \tag{13}$$

and

$$\boldsymbol{\sigma} = \frac{1}{L}\mathbf{p} \tag{14}$$

From eqs.(12) and (13), we obtain

$$\mathbf{v}_J\dot{\theta}_{J1} + \Delta_J\mathbf{f}_J\dot{\theta}_{J2} = (\mathbf{f}_J\times\boldsymbol{\rho}_{J3})\times\left[\dot{\boldsymbol{\sigma}} + \frac{1}{2}\dot{\phi}s(J)\mathbf{k}\times(\boldsymbol{\sigma}_I - \boldsymbol{\sigma}_{II})\right] \tag{15}$$

which can be written in vector form

$$\mathbf{A}_J\mathbf{t} = \mathbf{B}_J\dot{\boldsymbol{\gamma}}_J, \quad J = I, II \tag{16}$$

with the definitions below:

$$\mathbf{A}_J \equiv \left[\begin{array}{cc} \frac{1}{2}s(J)\boldsymbol{\Phi}_J\left[\mathbf{k}\times(\boldsymbol{\sigma}_I - \boldsymbol{\sigma}_{II})\right] & \boldsymbol{\Phi}_J \end{array}\right] \in \mathbb{R}^{3\times 2}, \quad \mathbf{B}_J \equiv \left[\begin{array}{cc} \mathbf{v}_J & \Delta_J\mathbf{f}_J \end{array}\right] \in \mathbb{R}^{2\times 4} \tag{17a}$$

$$\dot{\boldsymbol{\gamma}}_J \equiv \left[\begin{array}{c} \dot{\theta}_{J1} \\ \dot{\theta}_{J2} \end{array}\right], \quad \mathbf{t} \equiv \left[\begin{array}{c} \dot{\phi} \\ \dot{\boldsymbol{\sigma}} \end{array}\right], \quad \boldsymbol{\phi}_J \equiv \mathbf{f}_J\times\boldsymbol{\rho}_{J3} \tag{17b}$$

and $\boldsymbol{\Phi}_J$ is the *cross-product matrix* of vector $\boldsymbol{\phi}_J$ (Angeles, 2002).

Next, we consider both legs. Upon "stacking" the two corresponding kinematic relations derived from eq.(16), we obtain the kinematic relation for the whole system, namely,

$$\mathbf{A}\mathbf{t} = \mathbf{B}\dot{\boldsymbol{\theta}} \tag{18}$$

where the twist $\mathbf{t}$ was defined in eq.(17), the vector of active joint rates $\dot{\boldsymbol{\theta}}$, the *forward Jacobian* $\mathbf{A}$, and the *inverse Jacobian* $\mathbf{B}$ being defined, in turn, as

$$\dot{\boldsymbol{\theta}} \equiv \left[\begin{array}{c} \dot{\boldsymbol{\gamma}}_I \\ \dot{\boldsymbol{\gamma}}_{II} \end{array}\right] \in \mathbb{R}^4, \quad \mathbf{A} \equiv \left[\begin{array}{c} \mathbf{A}_I \\ \mathbf{A}_{II} \end{array}\right] \in \mathbb{R}^{6\times 4}, \quad \mathbf{B} \equiv \left[\begin{array}{cc} \mathbf{B}_I & \mathbf{O}_{32} \\ \mathbf{O}_{32} & \mathbf{B}_{II} \end{array}\right] \in \mathbb{R}^{6\times 4} \tag{19}$$

with $\mathbf{O}_{32}$ being the 3×2 zero matrix. Notice that the kinematic model (18) is *redundant*, for it entails six equations for four independent variables. Redundancy is introduced here to add *robustness* to the model. Robustness is needed to avoid *formulation singularities* (Ma and Angeles, 1992).

4.2 Singularity Analysis

The SMG meets a singular configuration whenever the 6×4 matrices $\mathbf{A}$ or $\mathbf{B}$ are rank-deficient. We thus have two types of singularities, namely, the *serial* singularities, and the *parallel* singularities. The former occurs when $\mathbf{B}$ is rank-deficient. In the presence of these singularities, there is a direction along which no Cartesian velocity can be produced. From eq.(19), $\mathbf{B}$ is rank-deficient when either $\mathbf{B}_I$ or $\mathbf{B}_{II}$ is rank-deficient. As a matter of fact, $\mathbf{B}_J$ loses rank if and only if

$$\mathbf{v}_J \parallel \mathbf{f}_J \tag{20a}$$

or

$$\Delta_J = 0 \tag{20b}$$

From eq.(10), $\mathbf{v}_J$ lies the plane spanned by vectors $\mathbf{k}$ and $\boldsymbol{\rho}_{J1}$, which is perpendicular to $\mathbf{f}_J$. Therefore, eq.(20a) holds if and only if

$$\mathbf{f}_J \times \boldsymbol{\rho}_{J3} \cdot \boldsymbol{\rho}_{J1} = 0 \tag{21a}$$

and

$$\mathbf{f}_J \times \boldsymbol{\rho}_{J3} \cdot \mathbf{k} = 0 \tag{21b}$$

On the one hand, eq.(21a) holds if $\boldsymbol{\rho}_{J3}$ is parallel to $\boldsymbol{\rho}_{J1}$, i.e., if points O_{J0}, O_{J2} and O_{J3} are aligned, as depicted in Fig. 7(a). On the other hand, eq.(21b) holds if $\boldsymbol{\rho}_{J3} \parallel \mathbf{k}$, i.e., if the distal link of leg J is vertical as depicted in Fig. 7(b).

Moreover, from eq.(11), eq.(20b) holds if and only if $\boldsymbol{\rho}_{J2}$ is parallel to $\boldsymbol{\rho}_{J3}$, i.e., leg J is fully extented, as illustrated in Fig. 7(c).

Parallel singularities, in turn, occur when $\mathbf{A}$ is rank-deficient. In the presence of these singularities, it is possible to move *locally* the operation point P with the actuators locked, the system thus resulting not in an isostatic structure, which should be the case, but in a mechanism, which cannot resist arbitrary loads, thereby becoming uncontrollable. To avoid any performance deterioration, it is necessary to have a Cartesian workspace free of parallel singularities.

From eq.(19), $\mathbf{A}$ loses rank if and only if its four columns are linearly dependent. From eq.(17) this happens when the nullspace of $\boldsymbol{\Phi}_I$, $\mathcal{N}(\boldsymbol{\Phi}_\mathcal{I})$, is identical to the nullspace of $\boldsymbol{\Phi}_{II}$, $\mathcal{N}(\boldsymbol{\Phi}_{\mathcal{II}})$. Since the two nullspaces are of dimension 1, and spanned, respectively by vectors $\boldsymbol{\Phi}_I$ and $\boldsymbol{\Phi}_{II}$, $\mathbf{A}$ loses rank when

$$\boldsymbol{\phi}_I = \pm\, \boldsymbol{\phi}_{II} \tag{22}$$

From eq.(17), eq.(22) is equivalent to

$$\mathbf{f}_I \times \boldsymbol{\rho}_{I3} = \pm\, \mathbf{f}_{II} \times \boldsymbol{\rho}_{II3} \tag{23}$$

In the case where the planes of legs I and II are parallel to each other, i.e., $\mathbf{f}_I = -\mathbf{f}_{II}$, eq.(23) holds if

$$\boldsymbol{\rho}_{I3} = \pm\, \boldsymbol{\rho}_{I3} \tag{24}$$

i.e., when segments $\overline{O_{I2}O_{I3}}$ and $\overline{O_{II2}O_{II3}}$ are both either vertical or horizontal, as illustrated in Figs. 8(a) and 8(b), respectively.

5 The Drive Units

The drive units of the robot deserve special attention, as their inertia plays a major role.

Each of the two identical units is to provide two independent motions, pan and tilt of the parallelogram links, and hence, independent rotations, one about a vertical axis, the pan, the other about a horizontal axis, the tilt. We want to produce each of these motions by the concurrent action of the two motors, in order to minimize the actuation-sensor complexity, and hence, to best distribute the load.

The drive units of the SMG are based on an innovative drive for the production of pan and tilt motions of a robotic link. The *Pan-Tilt Drive*, as the unit is referred to, is made up of one epicyclic gear train, which is driven by two grounded motors. Besides producing the *pan* motion through the rotation of the planet-carrier, two of their three planets are used to produce the *tilt* motion.

We could therefore use one motor in order to produce the pan motion and another one to produce the tilt motion. However, it is possible to use both motors again to produce the tilt motion. This can be achieved through the use of a differential gear train. As a result, with a suitable design, it is possible to use the full power of both motors for the two independent motions.

Figures 9(a) and 9(b) depict a schematic drawing and a 3D view of one of the two drive units of the manipulator, respectively. The drive units consist of the elements described below:

- The two motors M_A and M_B, mounted on a fixed frame (not shown in the figure) and driving gears 1 and 2, respectively, by means of the speed reducers GH_1 and GH_2;
- gear 1, meshing with gear 3, while gear 2 meshes with gear 4;
- an epicyclic train driven by the two motors: M_A drives the sun gear 5 while M_B drives the internal ring gear 7, these two gears meshing with the planets 6; when rotating about axis $\mathcal{A}_1$, these planets drive a planet carrier 8 rigidly attached to the housing of the whole mechanism and not included in the figures. The planet-carrier 8 produces the pan motion;
- two of the three identical planets, when rotating about their own axes of symmetry, produce the tilt motion;

The relations among the angular velocities are described by means of the notation below:

N_i: number of teeth of the i^{th} gear, for $i = 1, \ldots, 6$

$r_{3,1} = N_3/N_1 = N_4/N_2$: the gear ratio between gears 3 and 1, and between gears 4 and 2;

r_0: the reduction ratio from motor A (B) to gear 1 (2) through the gear head GH_1 (GH_2);

$r = r_0 r_{3,1}$: the total reduction ratio from the motors to the driven sun and ring gears;

$r_{6,5} = N_6/N_5$: the gear ratio between the planets 6 and the sun gear 5;

ω_i: angular velocity of the corresponding gears, or planet-carriers for $i = 1, \ldots, 6$;

ω_A: angular velocity of motor M_A;

ω_B: angular velocity of motor M_B;

ω_p: angular velocity of the pan motion, i.e., θ_{J1}, $J = I, II$;

ω_t: angular velocity of the tilt motion, i.e., θ_{J2}, $J = I, II$.

5.1 Forward Kinematics

We obtain here all the necessary relations between meshing gears, starting with the motors and ending with the relative velocity between the planet-carrier and the planets.

From the motors to the driven gears of the epicyclic train,

$$\omega_5 = -\frac{1}{r}\omega_A \tag{25a}$$

$$\omega_7 = -\frac{1}{r}\omega_B \tag{25b}$$

Inside the gear train, we have the well-known relations (Juvinall and Marshek, 2000)

$$\omega_8(N_5 + N_6) - \omega_6 N_6 = \omega_5 N_5 \tag{26a}$$

$$\omega_7(N_5 + 2N_6) = \omega_8(N_5 + N_6) + \omega_6 N_6 \tag{26b}$$

Dividing both sides of the above equations by N_5 and solving for ω_6 and ω_8, we obtain

$$\omega_6 = \frac{1}{2r_{6,5}}[-\omega_5 + (1 + 2r_{6,5})\omega_7] \tag{27a}$$

$$\omega_8 = \frac{1}{2(1 + r_{6,5})}[\omega_5 + (1 + 2r_{6,5})\omega_7] \tag{27b}$$

Substituting eqs.(25a) and (25b) into eqs.(27a) and (27b), while noticing that $\omega_p = \omega_8$ and $\omega_t = \omega_6 - \omega_8$ yields

$$\omega_p = -\frac{1}{2r(1 + r_{6,5})}[\omega_A + (1 + 2r_{6,5})\omega_B] \tag{28a}$$

$$\omega_t = \frac{1 + 2r_{6,5}}{2rr_{6,5}(1 + r_{6,5})}(\omega_A - \omega_B) \tag{28b}$$

Let us finally define $\boldsymbol{\omega}_{in}$ and $\boldsymbol{\omega}_{out}$ by

$$\boldsymbol{\omega}_{in} = \begin{bmatrix} \omega_A \\ \omega_B \end{bmatrix}, \boldsymbol{\omega}_{out} = \begin{bmatrix} \omega_p \\ \omega_t \end{bmatrix}$$

which are related by the drive-unit Jacobian $\mathbf{J}_D$ in the form

$$\boldsymbol{\omega}_{out} = \mathbf{J}_D \boldsymbol{\omega}_{in} \tag{29}$$

where $\mathbf{J}_D$ is defined as:

$$\mathbf{J}_D = \frac{1}{2r(1 + r_{6,5})} \begin{bmatrix} -1 & -(1 + 2r_{6,5}) \\ (1 + 2r_{6,5})/r_{6,5} & -(1 + 2r_{6,5})/r_{6,5} \end{bmatrix} \tag{30}$$

5.2 Inverse Kinematics

Regarding the control of the whole robot, a robot gesture is specified, for which the angular velocities of the two motors are required. These are readily obtained from the forward-kinematics relations, derived from eqs.(29) and (30).

Matrix $\mathbf{J}_D$ is invertible, its inverse being

$$\mathbf{J}_D^{-1} = -r \begin{bmatrix} 1 & -r_{6,5} \\ 1 & \dfrac{r_{6,5}}{1+2r_{6,5}} \end{bmatrix} \tag{31}$$

thereby deriving the inverse kinematics of the drive unit, namely,

$$\boldsymbol{\omega}_{in} = \mathbf{J}_D^{-1}\boldsymbol{\omega}_{out} \tag{32}$$

6 Dimensioning

The SMG is designed for pick-and-place operations based on the path defined to test the performance of SCARA robots, as depicted in Fig. 10. Moreover, one of the objectives of the project underlying this paper is to realize a parallel system that outperforms both serial SCARA systems and the parallel robots currently available for Schönflies motion generation, i.e., the H4 (Pierrot and Company, 1999), the T3-R1 (Gogu, 2004), and the fully isotropic parallel mechanisms developed by Carricato (2005). To this end, the design specifications for the McGill SMG are given below:

- The robot must be capable of producing a test cycle that is commonly accepted for SCARA systems, in at most 500 ms. The test cycle consists of:
  - 25-mm vertical displacement up
  - 300-mm horizontal displacement with a concomitant 180° turn
  - 25-mm vertical displacement down
  - 25-mm vertical displacement up
  - 300-mm horizontal displacement with a reversed 180° turn
  - 25-mm vertical displacement down
- The system is capable of attaining a configuration where kinetostatic robustness is achieved. As a matter of fact, from kinetostatics, the SMG is maximally accurate and robust when its forward and inverse Jacobians are maximally invertible, i.e., when their *condition number* κ is as small as possible.

The dimensions of the SMG are mainly determined by the isotropy conditions derived in the kinetostatic design, the geometric considerations, and the moveability of the end-effector to achieve the 180° rotation of the test cycle

One of the isotropy conditions derived in the kinetostatic design requires that $l_3 = \sqrt{2}R$ (Zhu, 2004). From geometric considerations, the radius R of the moving platform is equal to

200 mm, and hence, $l_3 = 282.843$ mm. R cannot be very large with respect to the dimensions of the test-cycle path, for this would render the manipulator bulky, and would also affect the moveability of the moving plate. If the R is too small, then the length of the distal links will be correspondingly reduced, but it cannot be too small; the manufacturing and assembly of the manipulator require the dimensions lie within the 1-meter scale.

The length of the proximal links is so determined that it would allow the maximum reach of the SMG to be at least 600 mm, which is the range of the Adept Cobra s600 (Adept, 2005); this length should lead to as low torques and forces as possible. Consequently, from the analysis presented in (Zhu, 2004), the optimal length of the proximal links turns out to be equal to 600 mm, i.e., $l_2 = 600$ mm.

7 Conclusions

In this paper an innovative robot, a Schönflies-Motion Generator, or SMG for brevity, capable of SCARA motions, was introduced. Its kinematics chain was described, which is based on two symmetric legs, each consisting of two Π-joints placed in series. Two proximal joints are driven by four motors installed on the base, producing pan and tilt motions of each leg. Two distal Π-joints are passive and follow the motion of the active ones. We found the singularities of the SMG. The design of the drive units, based on planetary gear trains, was discussed. The main expected advantages of the proposed design, with all motors fixed to the base and links, fabricated of a carbon fiber composite, are high performance speed and high positioning accuracy of the end platform.

Acknowledgments

This work was conducted with the support of the Idea to Innovation (I2I) program of Canada's Natural Sciences and Engineering Research Council (NSERC).

References

Adept (2005). Adept cobra s600. http://www.adept.com/products/details.asp?pid=7.

Angeles, J. (2002). *Fundamentals of Robotic Mechanical Systems: Theory, Methods, and Algorithms* (2 ed.). New York: Springer-Verlag.

Angeles, J. (2004). The qualitative synthesis of parallel manipulators. *ASME Journal of Mechanical Design 126*(4), 617–624.

Angeles, J. and A. Morozov (2003). A device for the production of schonflies motions. *International Patent Application*.

Bonev, I. (2003). The true origins of parallel robots. http://www.parallemic.org/Reviews/Review007.html.

Bottema, O. and B. Roth (1979). *Theoretical Kinematics*. Amsterdam: North Holland.

Brumson, B. (2005). Parallel kinematic robots. http://www.roboticsonline.com.

Carricato, M. (2005, May). Fully isotropic four-degrees-of freedom parallel mechanisms for schoenflies motion. *The International Journal of Robotics Research 24*(5), 397–414.

Gogu, G. (2004). *On Advances in Robot Kinematics*, Chapter Workspace and Isotropy: Fully-Isotropic T3R1-Type Parallel Manipulators, pp. 265–272. Kluwer Academic Publishers.

Hervé, J. (1999). The Lie group of rigid body displacements, a fundamental tool for mechanism design. *Mechanism and Machine Theory 34*, 719–730.

Juvinall, R. and K. Marshek (2000). *Fundamentals of Machine Component Design* (2 ed.). John Wiley & Sons.

Lapic (1994). Six-rod machining centers (tm series). http://www.lapic.ru.

Lee, C.-C. and J. Hervé (2005). On the enumeration of schoenflies motion generators. In *The Ninth IFToMM International Symposium on Theory of Machines and Mechanisms*, Bucharest, Romania.

Ma, O. and J. Angeles (1992). Architecture singularities of parallel manipulators. *The International J. Robotics & Automation 7*(1), 23–29.

Merlet, J. (2006). *Parallel Robots* (2 ed.). Solid Mechanics and Its Applications, Vol. 128. Springer. ISBN: 1-4020-4132-2.

Pierrot, F. and O. Company (1999). A new family of 4-dof parallel robots. In *IEEE/ASME International Conference on Advanced Intelligent Mechatronics*, Atlanta, USA.

Siciliano, B. (1999, June). The tricept robot: inverse kinematics, manipulability analysis and closed-loop direct kinematic algorithm. *Robotica 17*, 437–445.

Stewart, D. (1965). A platform with six degrees of freedom. In *Proc. Inst. Mech. Engineering*, Volume 180, London, pp. 371–386.

Yang, T., Q. Jin, and A. Liu (2001). Structure synthesis of 4-dof (3-translation and 1-rotation) parallel robot mechanisms based on the units of single-opened-chain. In *Proceedings of DETC'01, , ASME 2001 Design Engineering technical Conference*, Pittsburgh, PA.

Zhu, Y. (2004). The kinetostatic design of a novel parallel schönflies-motion generator. Master's thesis, Department of Mechanical Engineering & Centre for Intelligent Machines, McGill University.

List of Figures

Figure 1: An example of a parallel robot: Hexel R2000

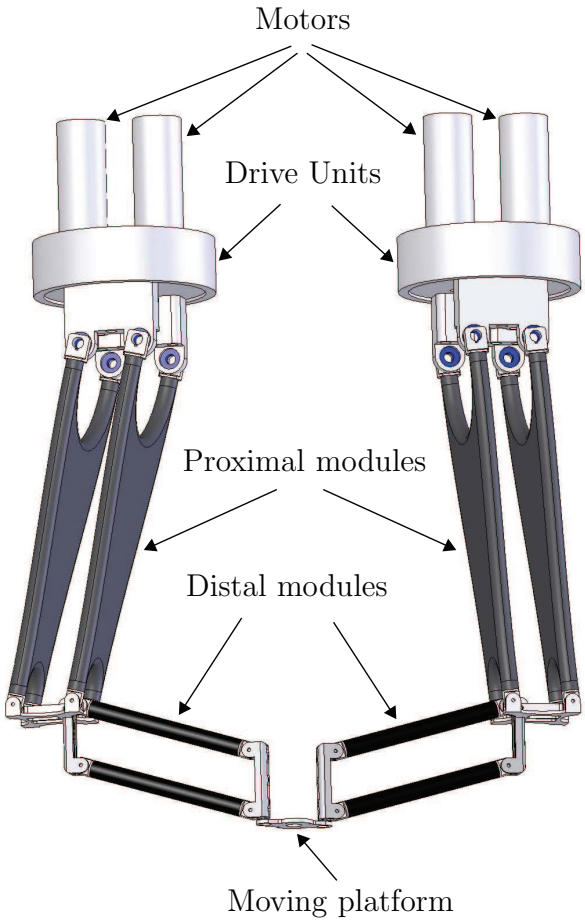

Figure 2: The McGill Schönflies-Motion Generator

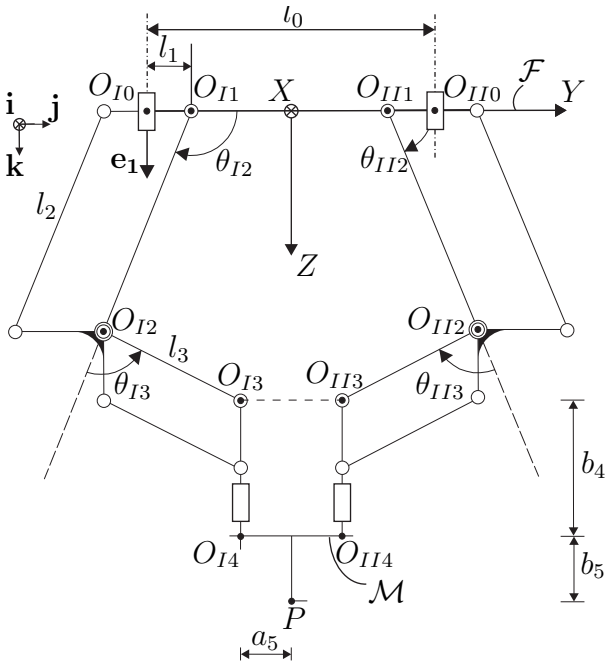

Figure 3: Kinematic chain of the parallel Schönflies-Motion Generator: front view

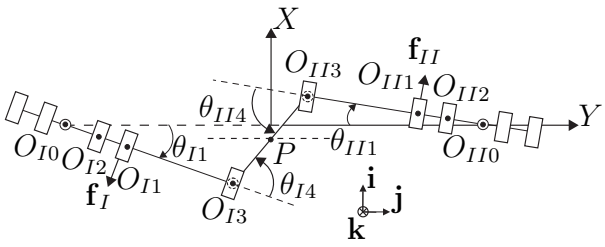

Figure 4: Kinematic chain of the parallel Schönflies-Motion Generator: top view

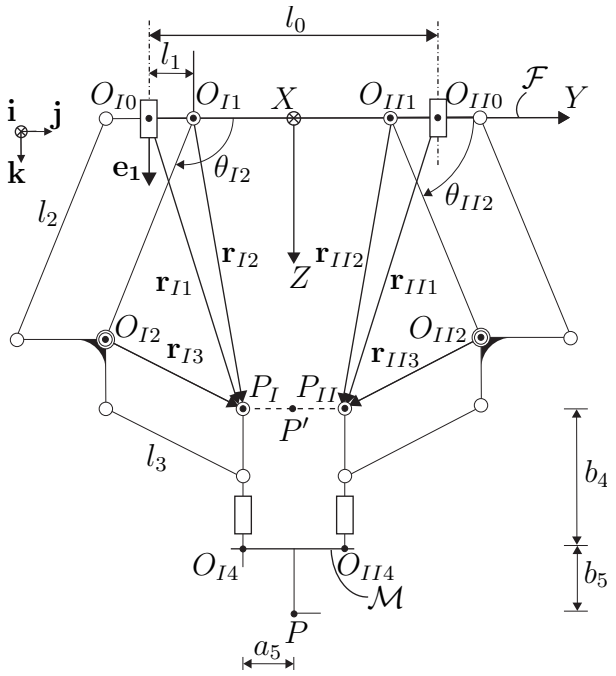

Figure 5: Vectors describing the kinematic chain of the parallel Schönflies-Motion Generator

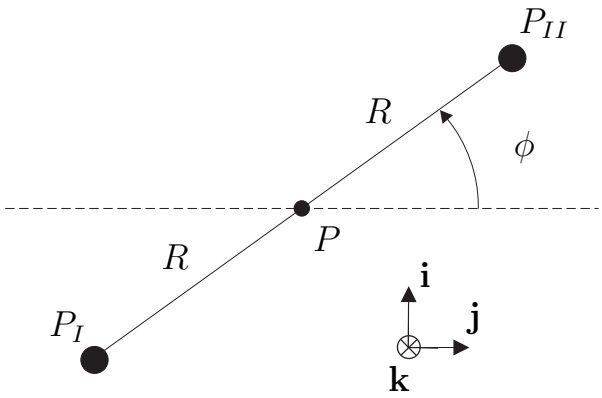

Figure 6: Top view of the moving plate in vector form

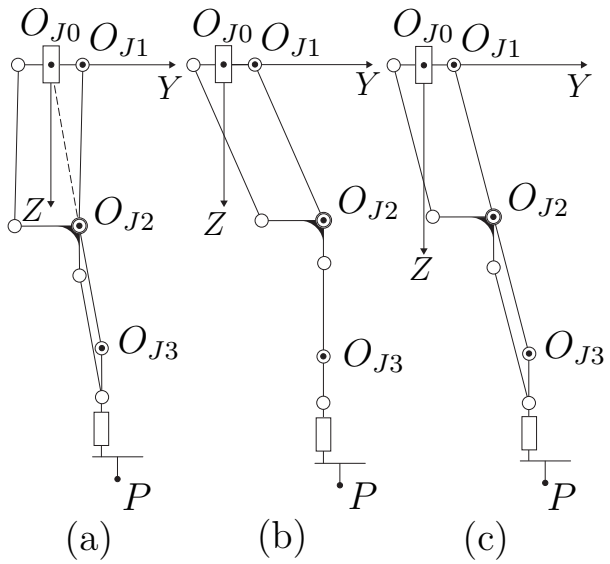

Figure 7: Three serial singular configurations

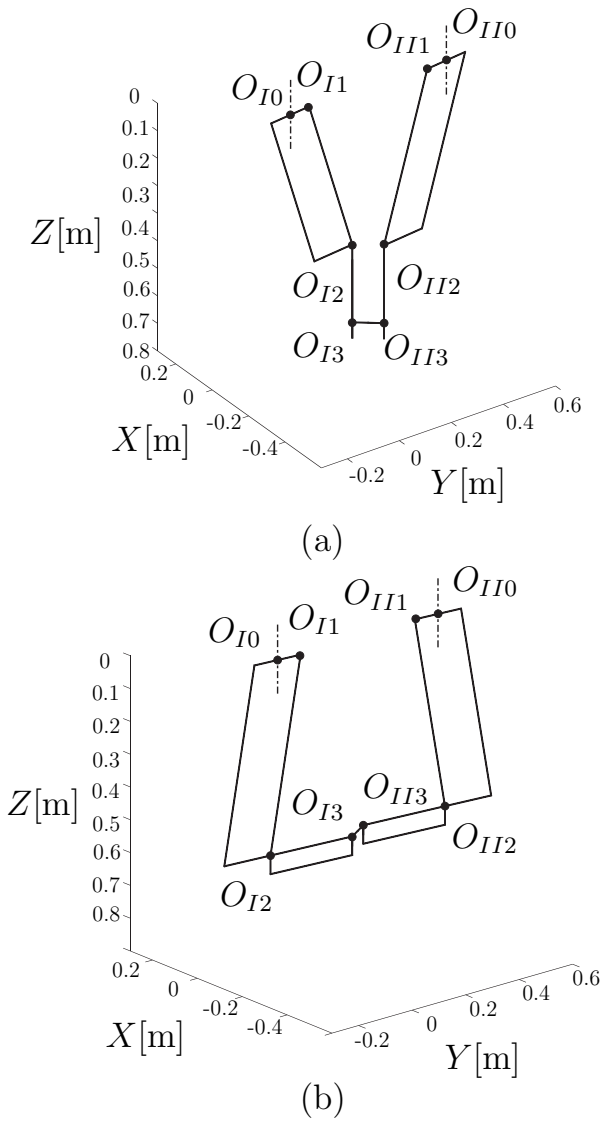

Figure 8: Two parallel singular configurations

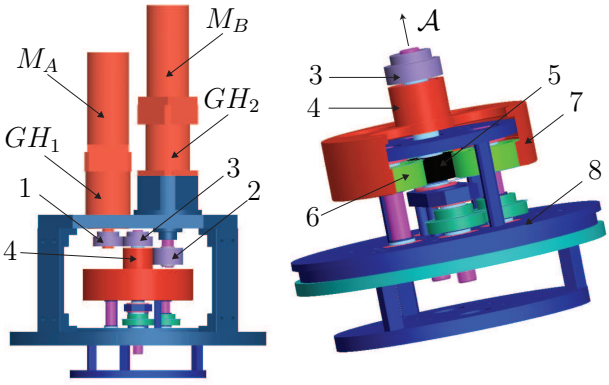

(a) (b)

Figure 9: The drive unit: (a) a global view, (b) the planetary gear train

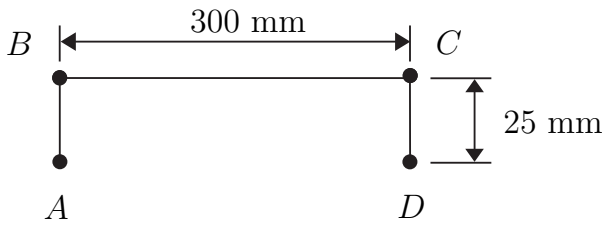

Figure 10: Path adopted for the manipulator design